Proceedings of ASME Turbo Expo 2020
Turbomachinery Technical Conference and Exposition
GT2020
September 21-25, 2020, Virtual, Online

GT2020-14413

CONSIDERATIONS ON AXIAL COMPRESSOR BLEED FOR SUB-IDLE PERFORMANCE MODELS

Ferran Roig Tió, Luis E. Ferrer-Vidal, Hasani Azamar Aguirre, Vassilios Pachidis

Centre for Propulsion, Cranfield University, Cranfield, Bedfordshire, UK

ABSTRACT

The trend towards increased bypass ratio and reduced core size in civil aero-engines puts a strain on ground-start and relight capability, prompting renewed interest in sub-idle performance modelling. While a number of studies have looked at some of the broad performance modelling issues prevalent in this regime, the effects that bleed can have on sub-idle performance have not been addressed in the literature. During start-up and relight, the unknown variation in bleed flows through open handling bleed valves can have a considerable impact on the compressor's operating line. This paper combines experimental, numerical and analytical approaches to look at the effect that sub-idle bleed flows have on predicted start-up operating lines, along with their effect on compressor characteristics. Experimental whole-engine data along with a purpose-built core-flow analysis tool are used to assess the effect of bleed model uncertainty on engine performance models. An experimental rig is used to assess the effects of reverse bleed on compressor characteristics and measurements are compared against numerical results. Several strategies for the generation of sub-idle maps including bleed effects are investigated.

Keywords: Compressor, bleed, sub-idle, locked-rotor, ground start, windmilling, performance, experiment, CFD, low-order model.

NOMENCLATURE

$1D$	One-dimensional
$3D$	Three-dimensional
CFD	Computational fluid dynamics
$ECMF$	Exit corrected mass flow
H	Total enthalpy
h	Specific total enthalpy
HP	High pressure
IP	Intermediate pressure
LP	Low pressure
LR	Locked-rotor
$M250$	Rolls-Royce Allison Model 250 engine
N	Spool speed
$Nref$	Reference spool speed
PR	Pressure ratio
Ps	Static pressure
Pt	Total pressure
R^2	Coefficient of determination
$R5$	Case with a bleed over the fifth rotor
$RANS$	Reynolds-averaged Navier-Stokes equations
$S1$	Case with a bleed over the first stator
SST	Menter's Shear Stress Transport turbulence model
Tt	Total temperature
TVD	Total variation diminishing method
U	Blade speed
W	Mass flow
WM	Windmilling
y^+	Wall coordinate

1. INTRODUCTION

Sub-idle refers to low-power operating points below the lowest power setting available to the operator. Operation below idle includes transient ground starts and relight manoeuvres. The former impacts start-up times and starter system design, while the latter is of paramount importance to aero-engine certification. Gas turbine thermodynamic matching models used for performance estimates rely on component data given in the form of performance characteristics. The lack of this data for operation below idle has traditionally meant that lower-fidelity models need to be used for sub-idle performance estimations. The low fidelity of these approaches has often caused costly re-designs to meet certification requirements as well as sub-optimal and over-engineered starter systems. With turbofan engine diameters increasing to improve specific fuel consumption, higher bypass ratios and smaller cores further strain a windmilling engine's ability to relight, due to comparatively lower mass flows available. The trend towards larger engine diameters thus leads to renewed interest in improved prediction capability for sub-idle operation, as evidenced from related literature in recent years [1-5].

Compressor sub-idle operation in particular has recently become more critical and received deserved attention [6-8]. As discussed in these sources as well as in [9], a compressor's sub-

idle performance map can be split into different regions depending on the sign of the work and pressure rise (Fig. 1). Aside from regular compressor operation with total pressure and enthalpy increase across the machine, a region exists where the total pressure across the machine decreases while total temperature still increases (known as stirrer or paddle operation) followed by a region where both total pressure and temperature fall across the machine (turbine operation). In between these last two regions, a locus of points can be defined where no enthalpy increase or drop occurs. This is the torque-free windmilling line, where the compressor rotates under the incoming flow but aerodynamic torque forces balance on the shaft. The changes in the sign of the enthalpy exchange have led to different performance parameter definitions being used for sub-idle performance. Since isentropic efficiency would become undefined for regions of zero work, the preferred approach is to replace this parameter with the torque. This parameter has been the one used in this work along with pressure ratio and corrected mass flow.

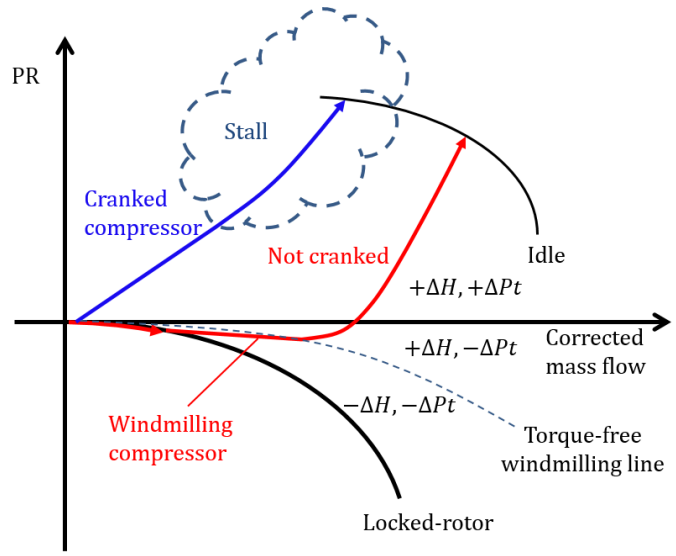

Fig. 1 Notional operating lines for cranked and uncranked compressors with compressor, stirrer and turbine regions.

The different regions present on a compressor pressure ratio vs corrected mass flow map are shown in Fig. 1 along with the notional operating lines of both cranked and uncranked compressors during a ground-start transient. As shown, compressors operate close to their stability limit during transients in the sub-idle region, and acceleration with partially stalled front stages at sub-idle speeds is not uncommon. Additionally, low stability margins make stall during a light-up an issue of outmost concern during development. These operability concerns lead to handling bleeds being actuated at low speeds, but while the schedules used may be well optimized for idle and above, their behaviour at very low sub-idle speeds is not fully understood.

While compressor sub-idle operation has been investigated previously, the bleed system's effect on overall compressor performance has received comparatively little attention. Most of the cases studied belong to the above idle region or deal with the proper computational modelling of bleeds [10-12]. More interestingly, Sexton had formerly suggested the importance of the bleed system at low speeds [13]. However, work in this field is even scarcer. Grimshaw studied bleed behaviour at low speeds but focused on the flow distortion it introduces to the main flow [14]. These studies have however not looked at the specific issue of compressor bleed behaviour at sub-idle, nor how to account for them in gas turbine performance models.

This paper first seeks to make a case for improved compressor bleed modelling at sub-idle. An experimental test bench is then introduced for the investigation of compressor reverse bleed operation. A numerical model is developed and performance results compared against experiment as well as a low-order compressor characteristics tool. The objectives are to develop low-order models capable of capturing the correct physics, present general trends that may be of interest to performance engineers, and to motivate further interest in compressor sub-idle bleed modelling.

2. BLEEDS & SUB-IDLE PERFORMANCE

Compressor inter-stage bleed at sub-idle can have important effects on the predicted performance obtained from ground start and relight models. During starts, compressor handling valves are typically opened to increase stability margin during light-up. Even if bleed valve settings are known, the resulting bleed flows are not necessarily known during starting transients, and these may actually switch in direction (into and out of the compressor) depending on the pressure gradient imposed on the bleed system at very low power settings. Due to instrumentation being designed for near-design point operation and the costs associated with having two sets of instruments, ground start measurement data are often not as reliable as would be required for a detailed analysis of flows through the engine core. To mitigate this problem, the core flows may be obtained indirectly from an analysis of measured data with the aid of compressor performance maps. However, without detailed knowledge of the bleed flows through the compressor, such approaches may yield different results depending on the bleed model used.

2.1 Bleed modelling in sub-idle performance models

Many techniques are available to account for compressor inter-stage bleed in whole-engine performance models relying on components maps. An approach is to correct the compressor outlet conditions to account for the enthalpy deficit arising from the extraction of a portion of the flow at a given thermodynamic state. When such a method is employed in a performance model, the bleed mass flow can be specified from a schedule as a fraction of the compressor inlet flow, or from a solution of the bleed system fluid network at the given conditions. The location of the bleed on the compressor determines the thermodynamic state (e.g. total temperature and pressure) of the bleed flow. This can be specified by fixing the fraction of work input that has been achieved up to the location of the bleed, along with the efficiency of the work input up to that point; this determines the bleed total

pressure and temperature. A simple way to specify this is to set the bleed offtake conditions by applying a specified fraction of the whole compressor's pressure and temperature rise. Near design point, the bleed offtake conditions may be well known from considerations of the compressor's axial work and flow distributions (i.e. knowledge of the stage matching and axial load and flow coefficients). However, as stage matching changes during off-design operation, accurate modelling would require the bleed work or total pressure fractions to be scheduled on the compressor's operating point. While modelling near design point could potentially assume the same total pressure and temperature fractions with minimal impact on accuracy, the greatly mismatched stages during sub-idle operation would preclude taking such an approach under those conditions. This is shown in Fig. 2, where the changes in work distribution both during sub-idle and near design are illustrated and compared.

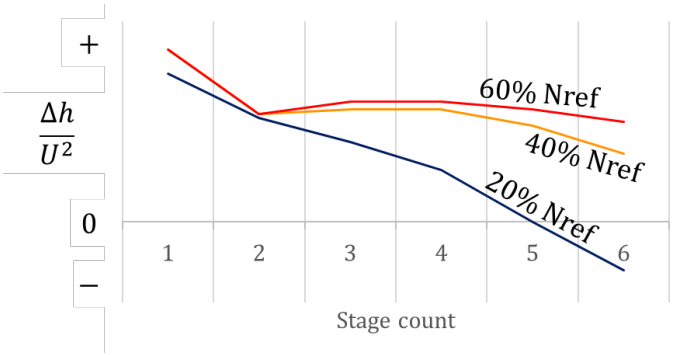

Fig. 2 Changes in stage matching for a 6-stage axial flow compressor analytical model during sub-idle (20% speed) and idle and above idle (40% and 60% speeds). The thermodynamic state of the flow entering a bleed near design when the corresponding stage is compressing may differ significantly from that during sub-idle when the stage could well be expanding (stages 5 and 6).

Another aspect of sub-idle performance that has previously been discussed is the need to use torque as a performance parameter instead of efficiency or enthalpy fraction definitions, as any performance representation considering enthalpy will run into issues at very low speed. This is due to no work being added to the flow at the torque-free point and at the zero-speed condition, causing the efficiency to become indeterminate. Similarly for bleed modelling, these considerations impact how the bleed outlet conditions are specified and their effects captured. While no work is done on the flow during locked-rotor operation, one can expect varying levels of bleed flow (in or out of the compressor) to impact the rotor torque and hence starting characteristics.

A way to alleviate the problem described here is to adopt a torque-based performance map representation where different maps are stacked on the level of bleed. This means a different compressor map is employed by the performance solver depending on the amount of bleed flow, with interpolation between different bleed maps as required. This approach would then capture the effect of stage mismatching at sub-idle, with the torque representation ensuring no region is undefined. However, this raises the concern of requiring large data sets to be generated, including sub-idle performance characteristics that capture the correct effects of bleed on pressure ratio and torque characteristics. This includes the case of reverse bleed operation, where sub-atmospheric conditions in the engine core may impose a pressure gradient in the opposite direction from what would normally be expected.

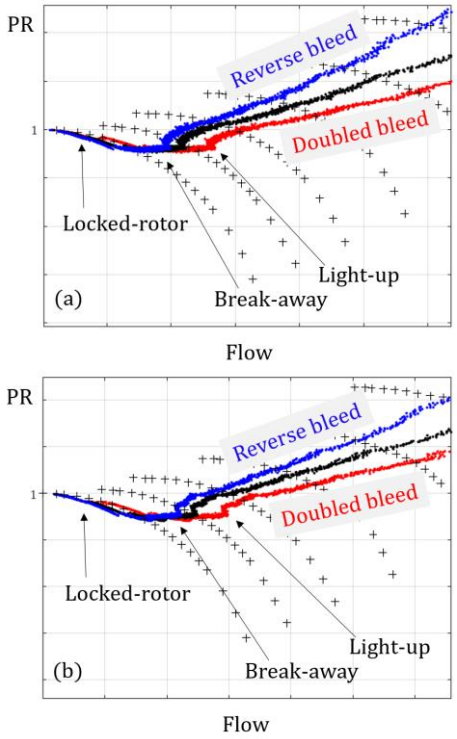

Fig. 3 Effect of representative notional bleed settings on ground start operating line of an HP compressor with low power start (a) and high power start (b). Untagged operating line (black) corresponds to baseline bleed setting.

2.2 Bleed modelling impact on sub-idle cases

In order to assess the impact that bleed modelling uncertainty may have, a core-flow analysis tool developed by the authors is used to calculate the core flow through the engine during ground starts. This tool makes use of limited measurement data and compressor maps to calculate the flow through the core compressors. Uncertainty in the bleed flows exists, so the effect of different bleed flow assumptions is investigated. Fig. 3 shows results from the analysis. In this case, results from two different starter motor powers on a multi-spool machine are analysed to obtain the operating line of the unpowered core HP compressor. Three different notional bleed cases are compared. A baseline case assuming certain amount of bleed flow obtained from standard bleed schedules is plotted along with two notional cases where this bleed flow is either doubled or applied in the reversed direction. Though such operation is unrealistic, as bleed flows would not be expected to remain constant during such a transient, this does allow us to understand the effect that uncertainties in the assumed bleed levels can have on the predicted performance.

We note that reversed bleed flows could potentially occur anytime a reversed pressure gradient (relative to nominal operation) is imposed on the secondary air system, even if the compressor is marginally compressing under sub-atmospheric inlet conditions.

Using test data with limited mass flow measurements, a comparison of the matching of the core-flow tool against test data using different bleed models can be made. Fig. 4 shows the different levels of matching obtained from test and model data using different bleed models. The first bleed model uses standard bleed schedules from near-nominal operation, while the second bleed model tries to account for changing bleed flows during the ground transient. While both models result in the same level of core-flow matching at idle speed, a difference is observed in the matching at low speed during the start: the first bleed model reaches errors in flow of up to 35% whereas the second bleed model produces errors in flow around 25%. This shows the impact that correct bleed modelling can have. Being able to predict core flows during start is very important for combustion chamber sizing, so this level of uncertainty in the predicted core-flows can have knock-on effects on combustion system design, often resulting in sub-optimal solutions.

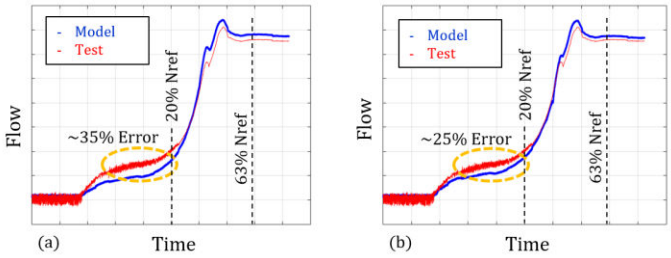

Fig. 4 Effect of representative bleed models on transient performance model matching against ground start test data. (a) Bleed modelled following nominal operation schedules. (b) Bleed modelled for ground start transient.

Aside from core-flow analysis for reliable ignition at light-up, bleed flows during relights can have non-negligible effects on required re-start times at altitude. Fig. 5 shows inflight windmill relight results from a three-shaft performance model developed by the authors. Increasing the amount of compressor bleed by 1% of the design point corrected inlet mass-flow for both the HP and IP compressors results in non-negligible effects on the transient acceleration of all three spools.

3. METHODS

The previous section presented a motivation for investigating the effects of compressor bleed at sub-idle. In order to investigate these effects a numerical model is developed to compare against experimental results of a compressor operating with a reverse bleed.

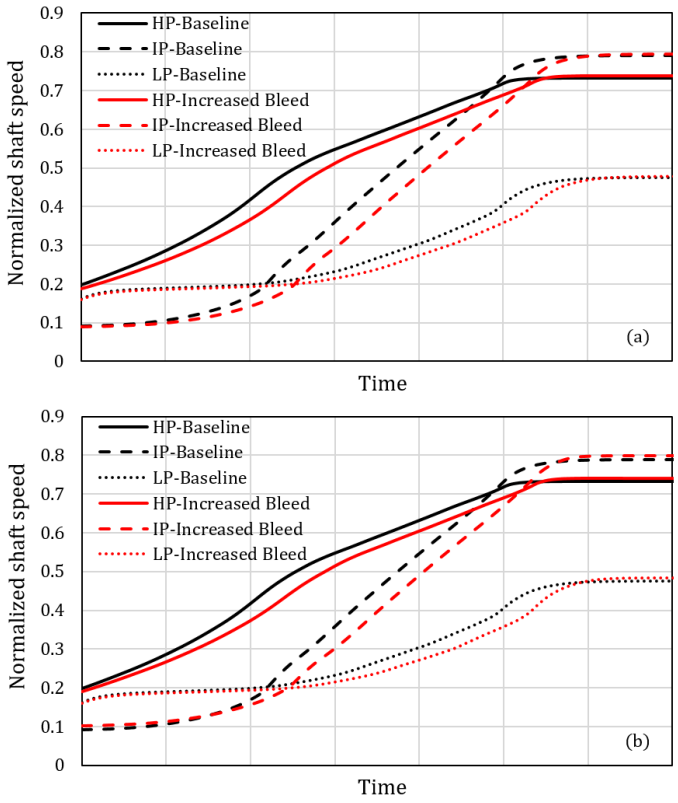

Fig. 5 Effect of different handling bleed valve settings on windmill relight prediction. (a) HP handling bleed increased by 1% design point corrected mass flow. (b) IP handling bleed increased by 1% design point corrected mass flow.

3.1 Numerical model

ANSYS CFX 19.1 is used as the flow solver. The 3D compressible Reynolds-Averaged Navier-Stokes (RANS) equations are solved. The turbulence model used is Menter's Shear Stress Transport (SST) [15]. The governing equations are linearized via a finite volume discretization using a co-located (non-staggered) grid (same grid for all transport equations). The CFX High Resolution scheme has been used. This scheme uses a proprietary blending between first order upwind and second order accurate discretization. Such a scheme will attempt a second order discretization but adjust the blending to first order upwind in order to satisfy a boundedness criterion. This results in a Total Variation Diminishing (TVD) scheme but also entails the solutions are not formally second order accurate through the domain [16].

The geometry has been provided by the industrial sponsor and validated against test-rig data. It has been meshed using ANSYS Turbogrid. A mesh sensitivity study has been performed to obtain the mesh sizing requirements. The study was performed using three different meshes with a uniform refinement ratio of ~1.5, achieving a mesh within the asymptotic range of convergence for pressure ratio and torque. All blade-row domains have been meshed with wall-function meshes and $y^+ \approx 30$ maintained throughout the domain. CFX scalable wall-functions have been used. The selected mesh sizes amount to

~0.5 million elements per blade-passage (~100 axial, ~70 circumferential, ~70 spanwise). The calculated Grid Convergence Index yields 0.12% for pressure ratio and 4.6% torque. The spatial order of convergence on torque is calculated as 1.88 while for pressure ratio it is merely 0.4, which is likely a consequence of the pressure ratio being insensitive to mesh size for the mesh sizes studied.

Boundary conditions to match experimental results (involving the axial part of a Rolls-Royce Allison Model 250 (M250) C20B compressor, see section 3.2) are total pressure inlet and mass flow outlet, with a mass flow inlet boundary condition on the bleed duct. The compressor rotor speed is set to match the one obtained from the experiment. This is shown in Fig. 6.

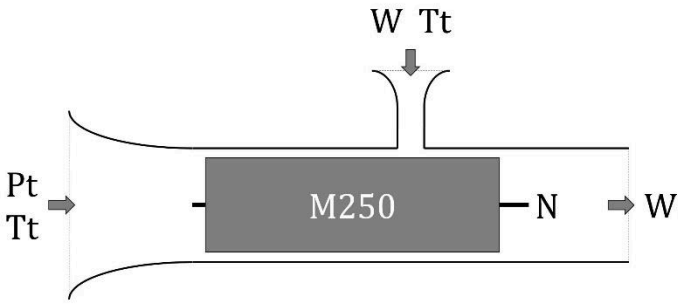

Fig. 6 Boundary conditions used in simulations for reproducing experimental results.

Pt and Tt are set to reference values of $1atm$ and $288.15K$ for all simulations. The values of the remaining boundary conditions are shown in Table 1. These values are taken from the experiment conditions and results presented below in Table 2.

Table 1 Boundary conditions used within the numerical analysis to reproduce the experimental results.

	Mass flow [Kg/s]	Bleed mass flow [Kg/s]	Spool speed [rpm]
Locked-rotor			
Bleed valve setting			
25% open	0.057	0.0059	0
	0.152	0.0153	0
100% open	0.013	0.0403	0
	0.127	0.0638	0
Windmilling			
Bleed valve setting			
25% open	0.060	0.0022	955
	0.234	0.0110	5520
100% open	0.038	0.0267	833
	0.198	0.0475	5053

In order to generate characteristics, an exit corrected mass flow (ECMF) boundary condition is used. This allows entire characteristics to be generated without needing to worry about switching the boundary condition between a static pressure outlet near choke and a mass flow outlet near stall [17]. This is shown in Fig. 7. All walls have been modelled as adiabatic no-slip boundary conditions.

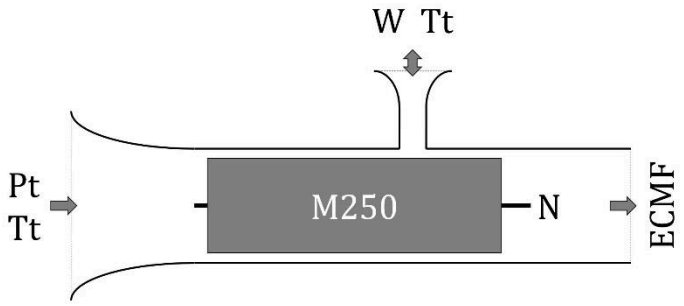

Fig. 7 Boundary conditions used in further simulations.

With such architecture, the spool speed has been chosen to simulate any characteristic of interest (from 0% at locked-rotor to ~60% for idle conditions). Bleed mass flow has been conveniently described as a percentage of inlet mass flow, either positive or negative, from −20% to 20%. Finally, a number of representative ECMF values has been set in each case to capture a significant part of the characteristic between stall and choke.

3.2 Experimental setup

An experimental test bench was commissioned to validate the CFD studies on bleed effect at sub-idle. This is an update of the rig described in [6]. The six-stage axial part of the same Rolls-Royce Allison Model 250 (M250) C20B compressor is used. This includes a bleed output over the fifth rotor.

The previous setup's instrumentation was capable of measuring inlet mass flow, pressure ratio and spool speed at any operating point, and torque in the locked-rotor case. A Venturi nozzle downstream of the compressor measures the outlet mass flow as well, which provides an indirect reading for the bleed mass flow through a simple subtraction. This Venturi nozzle, designed to British Standard BS EN ISO 5167, has been used to calibrate the inlet mass flow measurement through the inlet static pressure drop reading (Fig. 8).

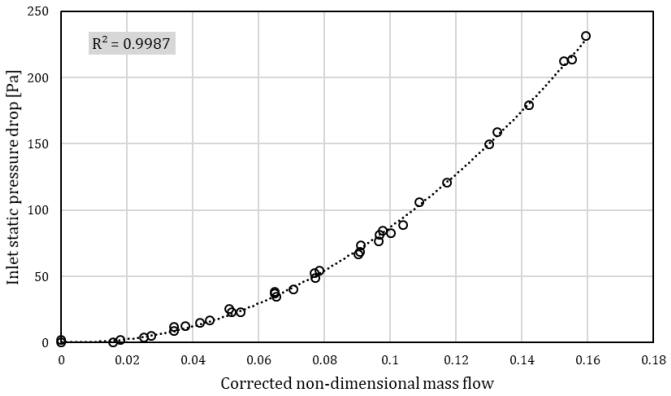

Fig. 8 Inlet pressure drop and mass flow correlation.

A downstream fan generates the flow by sucking air through the compressor. The experimental apparatus includes two control

valves. One valve is located upstream of the fan and controls the main flow. The other controls the bleed opening. The bleed output is open to ambient. This means that there is no additional control over the bleed system other than the bleed valve identified in Fig. 9.

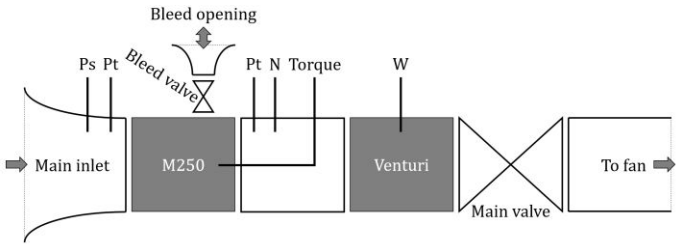

Fig. 9 Schematic illustration of sub-idle compressor bleed rig with its instrumentation.

The outlet mass flow is computed from measurements of static pressure in a Venturi nozzle. The inlet mass flow is computed from measurements of static pressure at the inlet per the calibration shown in Fig. 8. This method allows bleed mass flow both into and out of the compressor to be measured. The pressure ratio is computed from measurements of total pressure downstream and upstream of the compressor. Two Setra sensors and a Scanivalve pressure scanner carry out all these pressure readings. A static air source is used for reference pressure readings.

The torque is measured directly by a Novatech torque transducer and the spool speed is acquired with a Monarch Instruments optical speed sensor and a National Instruments digital counter, as they used to be in the previous setup.

This rig is able to simulate both locked-rotor and windmilling conditions. In the first case, the torque transducer is connected to the shaft, preventing it from spinning while measuring its torque. In the second case, the torque transducer is disassembled to allow the shaft to spin under the flow generated by the extraction fan. Since it will develop some torque to overcome the bearings' friction, these cannot be considered pure torque-free conditions, but are acceptable representative windmilling conditions.

3.3 Low-order map generation

The low-order model for sub-idle characteristics generation previously presented in [18] is used here to try to account for the effect of bleed on sub-idle performance. The model employs a mean-line analysis using empirical correlations for loss and deflection tailored to sub-idle [19]. The model accounts for bleed effects by simply breaking continuity in the velocity triangles and adding or subtracting flow as required. This simple approach would allow compressor performance maps including the effects of bleeds for locked-rotor and torque-free windmilling conditions to be effortlessly generated early in compressor design iterations. The ability to predict compressor characteristics with low-order models is required to ensure enough performance data are available early in the design process. This approach is tested against the experimental and numerical data to see if such a method can be relied upon to capture the pertinent bleed effects on performance at low speeds.

4. RESULTS

Results from the experimental test bench are first compared to the numerical results to derive relevant trends. These are later used to compare against a low-order characteristic generator. Finally, several strategies for the generation of sub-idle maps including bleed effects are investigated.

4.1 Numerical model

The experiment yielded data for several points of steady operation at locked-rotor and windmilling with different bleed valve openings. These same points were later simulated using the CFD model discussed in section 3.1. The results are presented and compared in Table 2.

The uncertainty of the measurements is represented by 1.96 times their standard deviation following the guidelines in [20]. The standard deviation is obtained from sets of 300 measurements. Results would lie within the stated range in 19 out of 20 times that this experiment were repeated.

A comment must be added concerning the largest error values on torque. These values are magnified by the fact that the value of torque in those cases is small. However, the absolute mismatch is of the same order as in all other cases. Therefore, the level of matching between numerical and experimental results are deemed acceptable for characteristics generation.

Table 2 Comparison of experimental and numerical results for locked-rotor and windmilling cases with bleed valve open 25% and 100%.

Mass flow [Kg/s]	Spool speed [rpm]	Pressure ratio [-]			Torque [Nm]		
		Experiment	CFD	Error	Experiment	CFD	Error
Locked-rotor							
Bleed valve 25% open							
0.057	0	0.9912 ± 0.0009	0.991	[−0.1%, 0.0%]	−0.1081 ± 0.0032	−0.126	[13%, 20%]
0.152	0	0.9391 ± 0.0057	0.937	[−0.8%, 0.4%]	−0.8288 ± 0.0145	−0.851	[1%, 5%]
Bleed valve 100% open							
0.013	0	0.9952 ± 0.0006	0.996	[0.0%, 0.2%]	−0.0588 ± 0.0031	−0.030	[−51%, −46%]
0.127	0	0.9395 ± 0.0065	0.930	[−1.6%, −0.3%]	−0.7520 ± 0.0154	−0.799	[4%, 8%]
Windmilling							
Bleed valve 25% open							
0.060	955	0.9959 ± 0.0003	0.995	[−0.1%, −0.1%]			
0.234	5520	0.9711 ± 0.0032	0.962	[−1.3%, −0.6%]			
Bleed valve 100% open							
0.038	833	0.9959 ± 0.0004	0.996	[−0.1%, 0.0%]			
0.198	5053	0.9700 ± 0.0033	0.962	[−1.2%, −0.5%]			

The locked-rotor and windmilling lines are in fact a small portion of the compressor map. Fig. 10 shows the results in terms of pressure ratio zoomed out from the actual M250 axial compressor map.

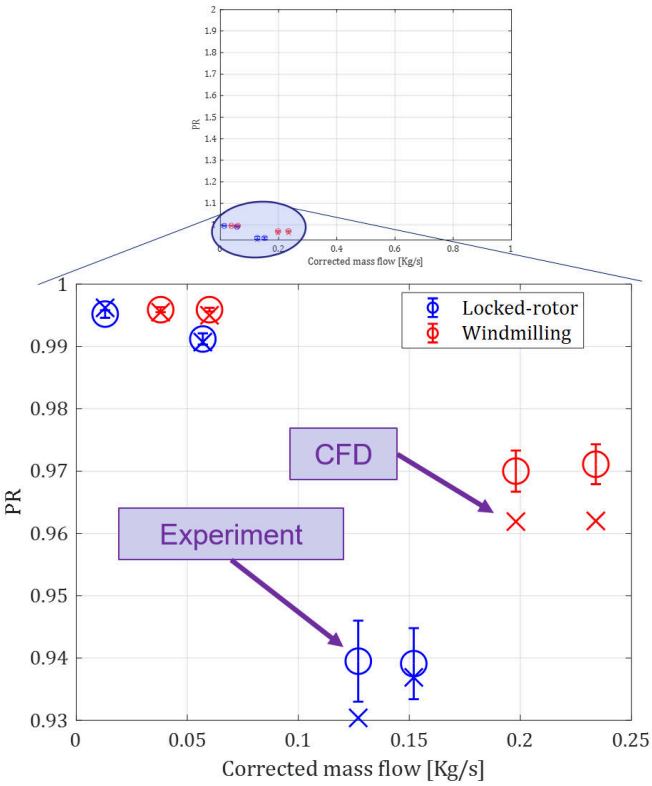

Fig. 10 Comparison of experimental and numerical results for locked-rotor and windmilling cases with different bleed valve opening.

The CFD model was used to derive compressor characteristics with different bleed settings. The boundary conditions were modified, as mentioned above (Fig. 7). The simulations reveal a shift in the characteristics. Taking the 40% speed line as an example (Fig. 11), with a bleed of 5% there is an average increase in mass flow of 3.1% along the characteristic. Similarly, a bleed of 20% results in a mass flow increase of 12.8%. Reverse bleeds show the same effect thus decreasing the mass flow along the characteristic. A reverse bleed of 5% results in a shift of −3.9% whereas a reverse bleed of 20% results in a shift of −13.7%. In terms of torque, the shift in the characteristic is less clear, but a proportional increase or decrease in mass flow can still be observed (Fig. 12).

The analysis above puts the focus on the effect of bleeds on overall mass flow, comparing points of identical pressure ratio. Yet, the opposite approach is equally interesting. The axial distribution of total pressure across the compressor is studied for different bleed settings (Fig. 13). These results explain the variation of pressure ratio for a fixed inlet mass flow. The evolution of total pressure is almost identical until the axial location where bleed mass flow is added to or extracted from the core mass flow. The variation in mass flow affects the total pressure drop over the fifth stator and consequently results in different total pressure rise and drop over the last rotor and stator respectively.

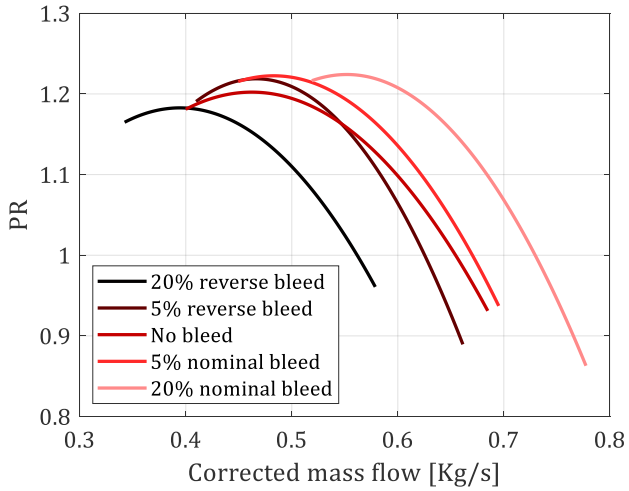

Fig. 11 Comparison of 40% speed line for different bleed mass flow percentages in terms of pressure ratio.

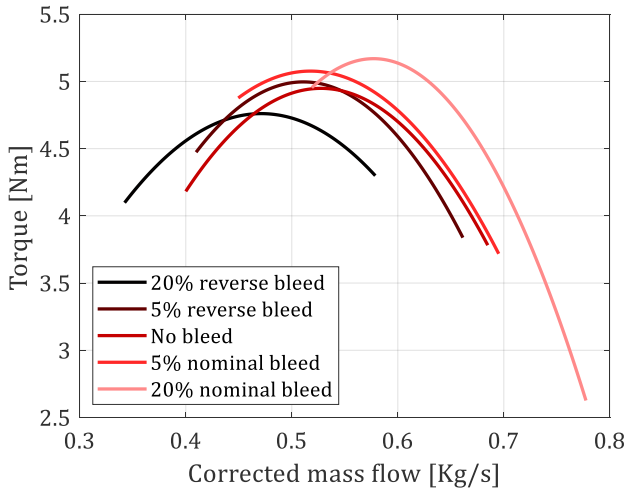

Fig. 12 Comparison of 40% speed line for different bleed mass flow percentages in terms of torque.

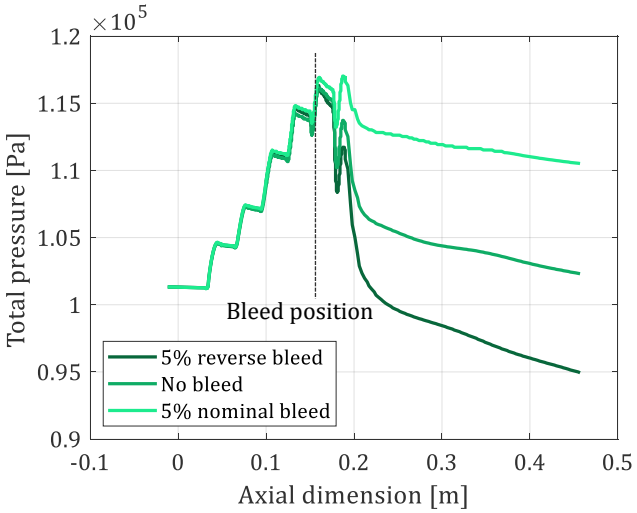

Fig. 13 Comparison of evolution of total pressure for identical cases with different bleed mass flow percentages.

4.2 Mean-line analysis

One way to generate compressor maps into sub-idle using limited data is through the calculation of locked-rotor and torque-free windmilling lines. These can be used to set the boundaries of the sub-idle regime, with interpolation used to generate further characteristics using any available above-idle data. Such an approach is discussed in [6] and can be implemented using a mean-line analysis or through-flow approaches [18]. In a mean-line analysis, the bleed can easily be implemented as a flow deficit that alters the velocity triangles. Fig. 14 compares the results from a low-order model against CFD results with bleed operating in both nominal and reversed direction. The map generator creates characteristics that match the numerical results. The root-mean-square deviation is less than 3% in terms of pressure ratio and less than 6% in terms of torque. This confirms that the low-order model can also be used to generate characteristics capturing the correct physics including bleeds at sub-idle.

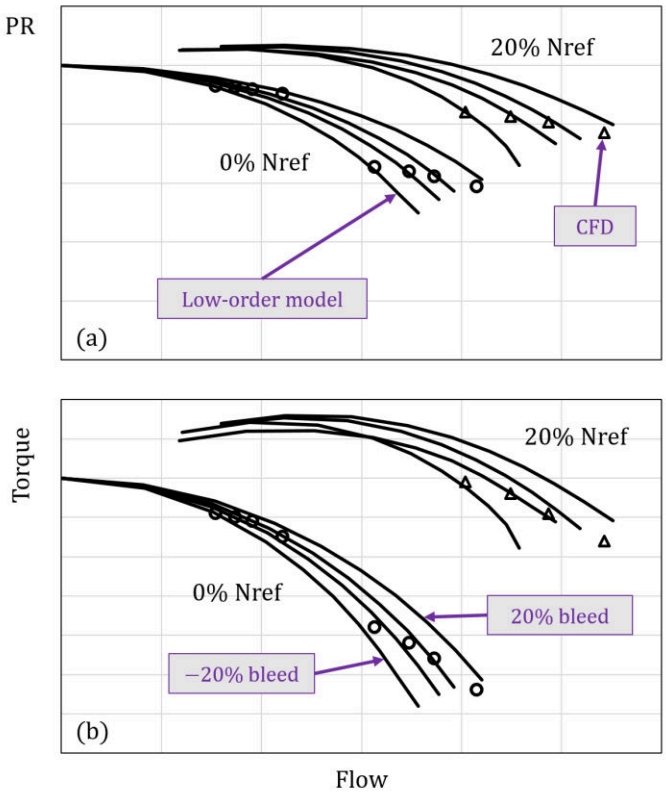

Fig. 14 Mean-line map generator (solid lines) vs 3D RANS CFD (symbols) for pressure ratio (a) and torque (b) characteristics of the M250 compressor with −20%, −5%, 5% and 20% bleed setting.

Different bleed positions along the compressor were also studied. The M250 compressor model was modified with a bleed over the first stator instead of its actual bleed over the fifth rotor. Several bleed settings, both nominal and reverse, were simulated under locked-rotor condition and compared to the characteristics generated by the low-order model (Fig. 15). The level of agreement is within the same range.

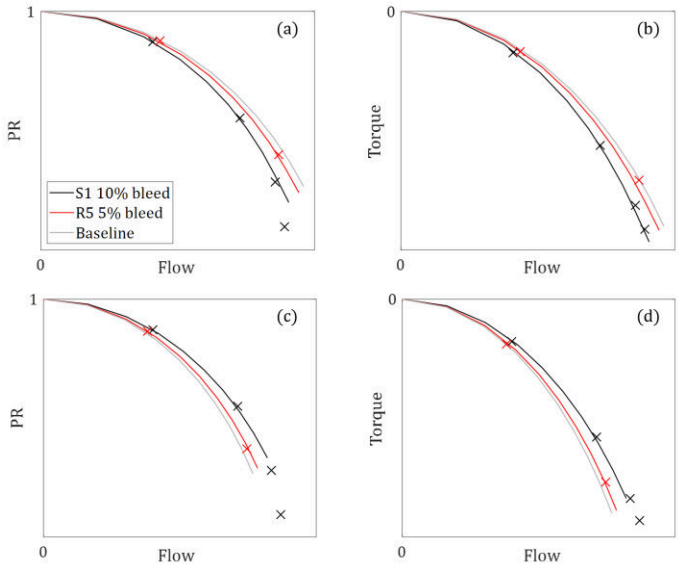

Fig. 15 Comparison of low-order model results (solid lines) and CFD results (symbols) for locked-rotor with different bleed location along the compressor and different bleed settings. (a) Reverse bleed and pressure ratio characteristics. (b) Reverse bleed and torque characteristics. (c) Nominal bleed and pressure ratio characteristics. (d) Nominal bleed and torque characteristics.

4.3 Map generation strategy

As mentioned above, [6] discusses sub-idle map generation through interpolation between calculated boundary lines and available above-idle data. The generation of the locked-rotor characteristic and the torque-free windmilling line accounting for both nominal and reverse bleeds has been covered in the previous section. The consequent interpolation process to generate a sub-idle map would require corresponding above-idle data, i.e. accounting for the same bleeds considered in the boundary lines generation. Nominal bleed effect is usually included in available engine data whereas reverse bleed is not.

Using real initial conditions from engine ground start data provided by the sponsor, three strategies were tested on a core-flow analysis tool. They are three different interpolation methods that generate three different sub-idle maps. Table 3 describes how each strategy accounts for reverse bleeds. For zero and nominal bleeds they proceed in the same usual way of calculating locked-rotor and windmilling lines accounting for the specified bleed and interpolating against corresponding above idle data.

Table 3 Different strategies to achieve a sub-idle map accounting for reverse bleeds.

Strategy	LR & WM lines	Sub-idle part	Above idle part
1	Calculated	Interpolated	Zero bleed
2	Calculated	Interpolated	Mirrored over zero bleed from nominal bleed data
3	Calculated	Calculated	Not needed

Fig. 16 illustrates the different strategies and their approach to getting a sub-idle map accounting for reverse bleeds.

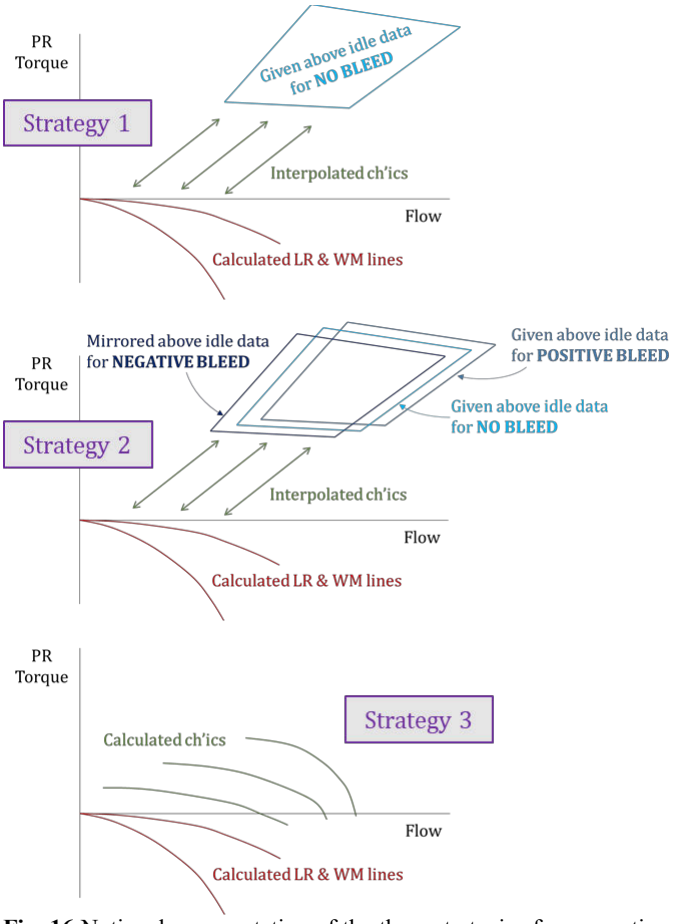

Fig. 16 Notional representation of the three strategies for generating a sub-idle map accounting for reverse bleeds that were studied.

Results show that the operating lines predicted using the three different maps fall into a very similar place (Fig. 17). In short, the strategy used has no significant impact to the performance prediction. Strategy 2 involves few mathematical manipulation of the above idle data. In addition, strategy 3 is thought to be less accurate because it uses a mean-line analysis tailored to locked-rotor and windmilling speeds, hence unsuitable for higher speeds. Therefore, strategy 1 should be used in any case.

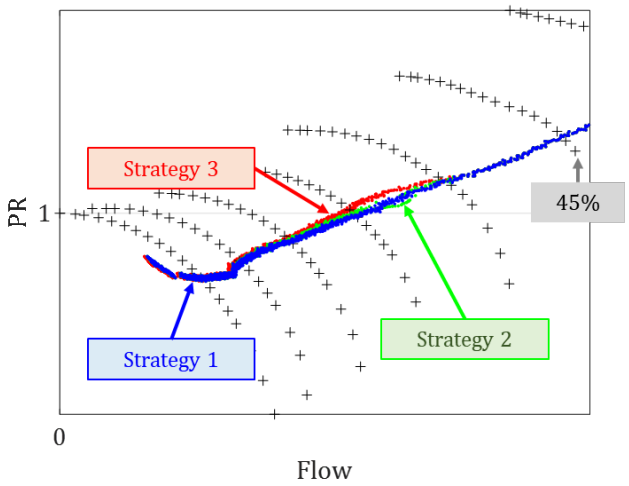

Fig. 17 Operating lines during a ground start (sub-idle region). Three operating lines are displayed: blue for strategy 1, green for strategy 2 and red for strategy 3. A map is shown in the background just for reference, note that each operating line uses several and different maps based on the bleed setting and the strategy followed.

5. CONCLUSIONS

The effects that inter-stage bleeds may have on whole-engine performance models at sub-idle were investigated first. The uncertainty caused by lack of knowledge of these effects motivates the need for methods to capture them on the component maps that populate performance models.

Results from a CFD model are compared against in-house experimental results and used to evaluate the effects of bleed on axial compressor sub-idle performance. A low-order model to predict this same bleed effect on axial compressor sub-idle performance has been shown to correctly capture the trends through the application of a mean-line analysis using a set of correlations available in the literature. This low-order model takes into account the compressor geometry parameters and the bleed axial position, allowing sub-idle performance characteristics to be obtained for compressors with inter-stage bleed offtakes. This allows the generation of accurate sub-idle maps with representative bleed mass flow settings.

ACKNOWLEDGEMENTS

We would like to thank Rolls-Royce plc. for encouraging this research and allowing its publication. The authors are indebted to Richard Tunstall, Mark Stockwell and Steven Brown for their continued support of sub-idle performance modelling efforts. The authors would also like to thank Mark McLaren for his assistance in securing compressor geometry and performance data for validation.

REFERENCES

[1] I. Fuksman and S. Sirica (2012). Modeling of a turbofan engine start using a high fidelity aerothermodynamic simulation. *Proceedings of the ASME Turbo Expo*, vol. 1, pp. 459–466. Copenhagen, Denmark.

[2] S. Bretschneider and J. Reed (2016). Modeling of start-up from engine-off conditions using high fidelity turbofan engine simulations. *Journal of Engineering for Gas Turbines and Power*, vol. 138, n. 5.

[3] Z. Hu, B. Jiang, J. Wang and X. He (2017). A generalized method for sub-idle modeling of aircraft engines. *8th International Conference on Mechanical and Aerospace Engineering*, pp. 527–531. Prague, Czech Republic.

[4] A. Ferrand, M. Bellenoue, Y. Bertin, R. Cirligeanu, P. Marconi and F. Mercier-Calvairac (2018). High fidelity modeling of the acceleration of a turboshaft engine during a restart. *Proceedings of the ASME Turbo Expo*, vol. 1. Lillestrøm (Oslo), Norway.

[5] J. W. Chapman, A. J. Hamley, T.-H. Guo and J. Litt (2016). Extending the operational envelope of a turbofan engine simulation into the sub-idle region. *AIAA Atmospheric Flight Mechanics Conference*. San Diego, California, USA.

[6] L. E. Ferrer-Vidal, V. Pachidis and R. J. Tunstall (2018). An enhanced compressor sub-idle map generation method. *Proceedings of GPPS Forum 2018*. Zurich, Switzerland.

[7] M. Nocture, Y. Mery, J. Ruiz Domingo, N. Rochuon, B. Bonnal, E. Vanoli, P. Gopalakrishnan and A. Jammalamadaka (2019). Study of high pressure compressor performances in windmilling conditions by three complementary approaches: experiment, LBM and 1D modelling. *Proceedings of the ASME Turbo Expo*. Phoenix, Arizona, USA.

[8] J. Kurzke (2019). Generating compressor maps to simulate starting and windmilling. *ISABE 2019*. Canberra, Australia.

[9] P. P. Walsh and P. Fletcher (2004). *Gas Turbine Performance*.

[10] S. Lück, S. Kuntzagk, G. Doebbener, A. Kellersmann, C. Bode and J. Friedrichs (2019). Accuracy assessment of steady and unsteady multistage high pressure compressor simulations. *Proceedings of the ASME Turbo Expo*. Phoenix, Arizona, USA.

[11] F. Conan, S. Savarese and S. Moteurs (2001). Bleed airflow CFD modeling in aerodynamics simulations of jet engine compressors. *Proceedings of the ASME Turbo Expo*, vol. 1. New Orleans, Louisiana, USA.

[12] G. Cerri, C. Salvini, R. Procacci and F. Rispoli (1993). Fouling and air bleed extracted flow influence on compressor performance. *ASME International Gas Turbine and Aeroengine Congress and Exposition*, vol. 3C. Cincinnati, Ohio, USA.

[13] W. R. Sexton (2001). *A Method to Control Turbofan Engine Starting by Varying Compressor Surge Valve Bleed*. MSc thesis. Virginia Polytechnic Institute and State University.

[14] S. D. Grimshaw, G. Pullan and T. Walker (2015). Bleed-induced distortion in axial compressors. *Journal of Turbomachinery*, vol. 137, n. 10.

[15] F. R. Menter (1994). Two-Equation Eddy-Viscosity Turbulence Models for Engineering Applications. *AIAA Journal*, vol. 32, n. 8.

[16] ANSYS Inc. (2016). *ANSYS CFX Theory Guide*.

[17] ANSYS Inc. (2016). *ANSYS CFX Reference Guide: CFX Best Practices Guide for Turbomachinery*.

[18] M. Righi, L. E. Ferrer-Vidal, A. Allegretti and V. Pachidis (2019). Low-order models for the calculation of compressor sub-idle characteristics. *ISABE 2019*. Canberra, Australia.

[19] L. E. Ferrer-Vidal, M. Schneider, A. Allegretti and V. Pachidis (2019). A loss and deflection model for compressor blading at high negative incidence. *Journal of Turbomachinery*, pp. 1–19.

[20] R. J. Moffat (1988). Describing the Uncertainties in Experimental Results. *Experimental Thermal and Fluid Science*, vol. 1, n. 1.